

SI Guide

Negative feedback control of neuronal activity by microglia

Ana Badimon^{1,2,3}, Hayley J. Strasburger^{1,2,3}, Pinar Ayata^{1,2,3,4}, Xinhong Chen⁵, Aditya Nair⁵, Ako Ikegami^{6,7}, Philip Hwang^{1,2,3}, Andrew T. Chan^{1,2,3}, Steven M. Graves⁸, Joseph O. Uweru⁹, Carola Ledderose¹⁰, Munir Gunes Kutlu¹¹, Michael A. Wheeler¹², Anat Kahan⁵, Masago Ishikawa¹, Ying-Chih Wang¹³, Yong-Hwee E. Loh¹, Jean X. Jiang¹⁴, D. James Surmeier¹⁵, Simon C. Robson^{16,17}, Wolfgang G. Junger¹⁰, Robert Sebra¹³, Erin S. Calipari^{11,18,19,20,21}, Paul J. Kenny¹, Ukpong B. Eyo⁹, Marco Colonna²², Francisco J. Quintana^{12,23}, Hiroaki Wake^{6,7}, Viviana Gradinaru⁵ & Anne Schaefer^{1,2,3,4}

¹Nash Family Department of Neuroscience, Icahn School of Medicine at Mount Sinai, New York, NY, USA.

²Department of Psychiatry, Icahn School of Medicine at Mount Sinai, New York, NY, USA.

³Center for Glial Biology, Icahn School of Medicine at Mount Sinai, New York, NY, USA.

⁴Ronald M. Loeb Center for Alzheimer's Disease, Icahn School of Medicine at Mount Sinai, New York, NY, USA.

⁵Division of Biology and Biological Engineering, California Institute of Technology, Pasadena, CA, USA.

⁶Department of Anatomy and Molecular Cell Biology, Nagoya University Graduate School of Medicine, Nagoya, Japan.

⁷Division of System Neuroscience, Kobe University Graduate School of Medicine, Kobe, Japan.

⁸Department of Pharmacology, University of Minnesota, Minneapolis, MN, USA.

⁹Center for Brain Immunology and Glia, Department of Neuroscience, University of Virginia, Charlottesville, VA, USA.

¹⁰Department of Surgery, Beth Israel Deaconess Medical Center, Harvard Medical School, Boston, MA, USA.

¹¹Department of Pharmacology, Vanderbilt University, Nashville, TN, USA.

¹²Ann Romney Center for Neurologic Diseases, Brigham and Women's Hospital, Harvard Medical School, Boston, MA, USA.

¹³Department of Genetics and Genomic Sciences, Icahn Institute of Data Science and Genomic Technology, Icahn School of Medicine at Mount Sinai, New York, NY, USA.

¹⁴Department of Biochemistry and Structural Biology, University of Texas Health Science Center, San Antonio, TX, USA.

¹⁵Department of Physiology, Feinberg School of Medicine, Northwestern University, Chicago, IL, USA.

¹⁶Department of Anesthesia, Beth Israel Deaconess Medical Center and Harvard Medical School, Boston, MA, USA.

¹⁷Department of Medicine, Beth Israel Deaconess Medical Center and Harvard Medical School, Boston, MA, USA.

¹⁸Vanderbilt Brain Institute, Vanderbilt University, Nashville, TN, USA.

¹⁹Vanderbilt Center for Addiction Research, Vanderbilt University, Nashville, TN, USA.

²⁰Department of Molecular Physiology and Biophysics, Vanderbilt University, Nashville, TN, USA.

²¹Department of Psychiatry and Behavioral Sciences, Vanderbilt University, Nashville, TN, USA.

²²Department of Pathology and Immunology, Washington University School of Medicine, St. Louis, MO, USA.

²³The Broad Institute of MIT and Harvard, Cambridge, MA, USA.

Table of Contents:

Supplementary Figure 1

Original western blots for data shown in Fig. 4e, Extended Data Fig. 3f, and Extended Data Fig. 5g. (PDF file)

Supplementary Figure 2

Original western blots for data shown in Extended Data Fig. 7f, and Extended Data Fig. 8d, and 8j. (PDF file)

Supplementary Figure 3

Gating strategy for Fig. 4b. (PDF file)

Supplementary Figure 4

Gating strategy for Extended Data Fig. 7b. (PDF file)

Supplementary Figure 5

Gating strategy for Extended Data Fig. 7d. (PDF file)

Supplementary Table 1

Genes enriched in microglia upon neuronal activation (DESeq2 analysis) (Excel table)

Supplementary Table 2

Genes enriched in microglia upon neuronal inhibition (DESeq2 analysis) (Excel table)

Supplementary Table 3

Genes enriched in D1 neurons in striatum of *Il34^{fl/fl}Drd1a^{Cre/+}* (DESeq2 analysis) (Excel table)

Supplementary Video 1

Representative field of view for live imaging of calcium transients in striatal neurons for data shown in Figure 3a-f and Extended Data Figure 6a-g. (AVI file)

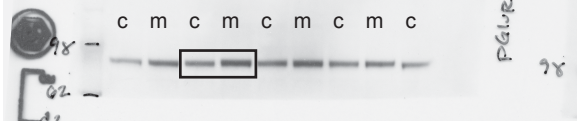
Supplementary Video 2

Representative field of view for live imaging of microglia (green) contact with neuronal terminals (red) for data shown in Figure 3g-h and Extended Data Figure 6h-j. Scale bar = 20 μ M. (AVI file)

Supplementary Figure 1

Fig 4e

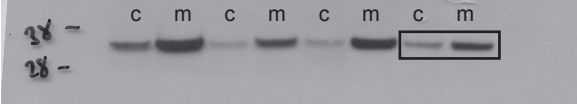
phosGLUR1Ser845; *Il34^{fl/fl}* (c) and *Il34^{fl/fl}Drd1a^{Cre/+}* (m)



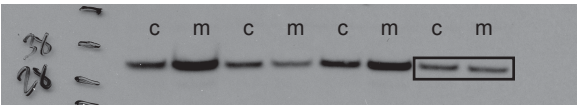
GLUR1; *Il34^{fl/fl}* (c) and *Il34^{fl/fl}Drd1a^{Cre/+}* (m)



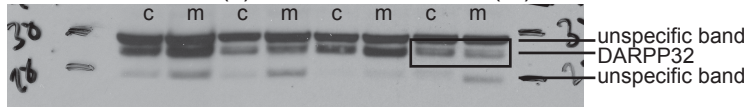
phosDARPP32Thr34; *Il34^{fl/fl}* (c) and *Il34^{fl/fl}Drd1a^{Cre/+}* (m)



phosDARPP32Thr75; *Il34^{fl/fl}* (c) and *Il34^{fl/fl}Drd1a^{Cre/+}* (m)

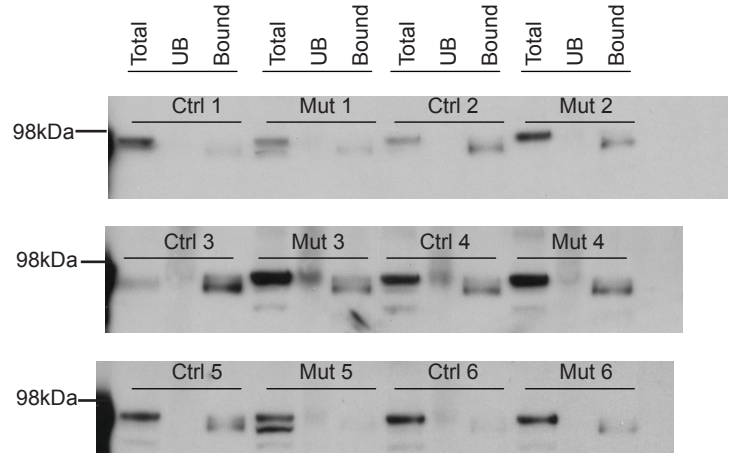


DARPP32; *Il34^{fl/fl}* (c) and *Il34^{fl/fl}Drd1a^{Cre/+}* (m)



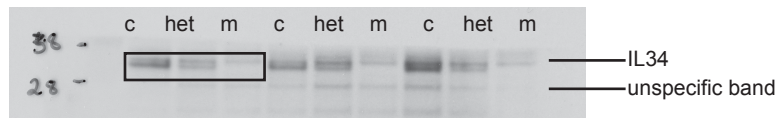
Extended Data Fig. 5g

DRD1 in total lysate, unbound (UB) and bound (biotinylated) striatal slices in *Il34^{fl/fl}* (ctrl) and *Il34^{fl/fl}Drd1a^{Cre/+}* (mut)

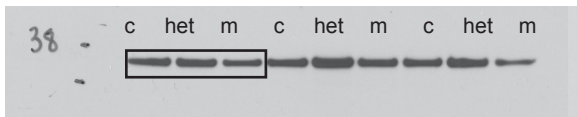


Extended Data Fig 3f

IL34; *Il34^{fl/fl}*(C), *Il34^{fl/+}Nestin^{Cre/+}* (Het); *Il34^{fl/fl}Nestin^{Cre/+}* (m) samples



DARPP32; *Il34^{fl/fl}*(C), *Il34^{fl/+}Nestin^{Cre/+}* (Het); *Il34^{fl/fl}Nestin^{Cre/+}* (m) samples



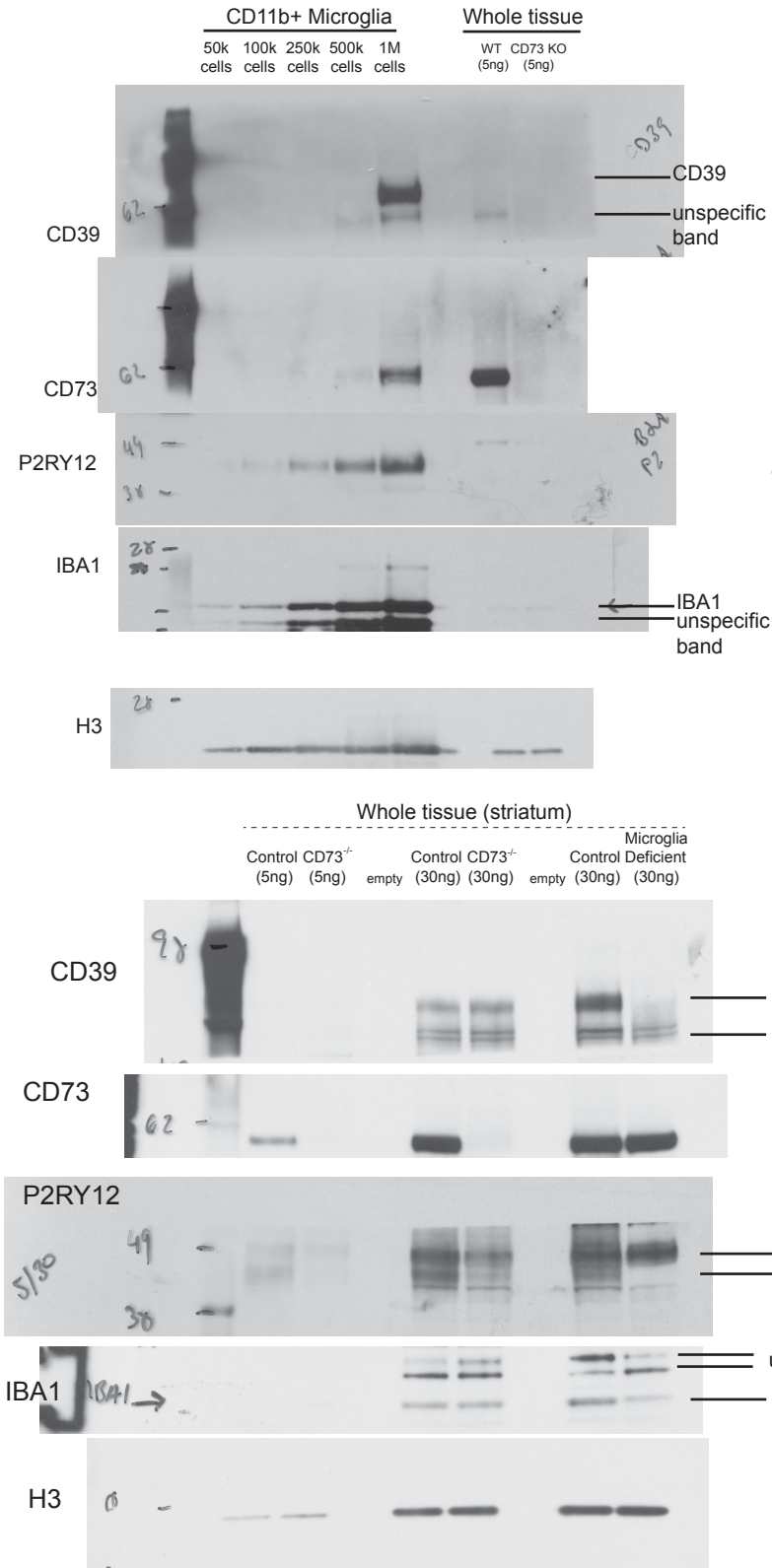
Original western blots

Cropped KODAK films for Western blots in Fig. 4e, Extended Data Fig. 3f, and Extended Data Fig. 5g are shown. Membranes were cut prior to antibody staining to allow for simultaneous detection of proteins running at different sizes on the same membrane.

Supplementary Figure 2

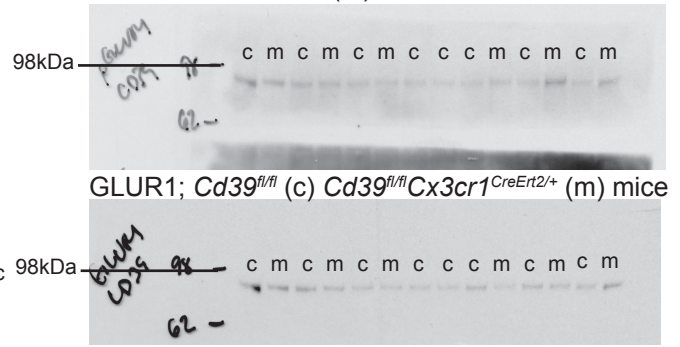
Extended Data Fig. 7f

CD11b⁺ isolated microglia (wild type mice)
and whole tissue (wild type and Nt5e/CD73^{-/-})



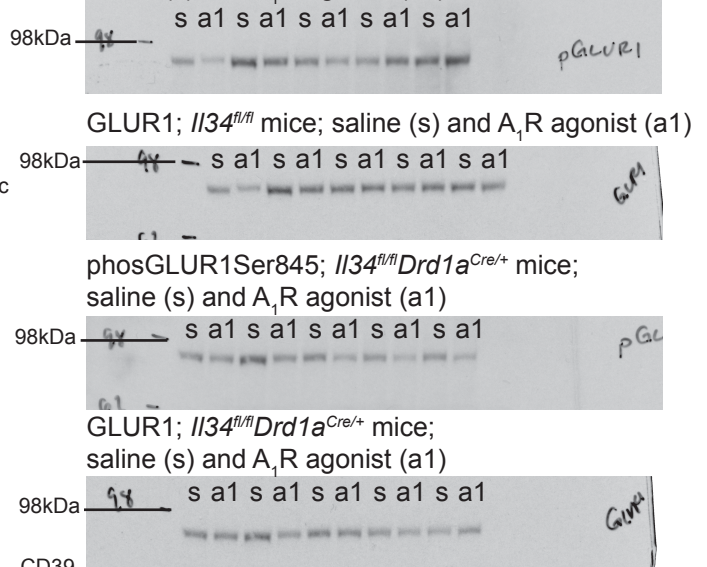
Extended Data Fig. 8d

phosGLUR1Ser845; *Cd39^{fl/fl}* (c) and
Cd39^{fl/fl}Cx3cr1^{CreErt2/+} (m) mice



Extended Data Fig. 8j

phosGLUR1Ser845; *Il34^{fl/fl}* mice;
saline (s) and A₁R agonist (a1)



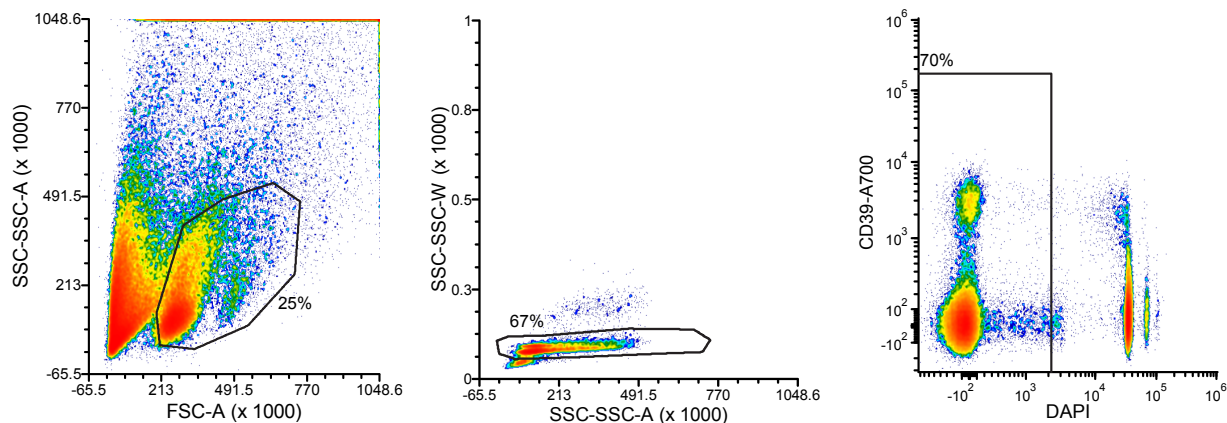
Original western blots

Cropped KODAK films for Western blots in Extended Data Fig. 7f, 8d, and 8j are shown.

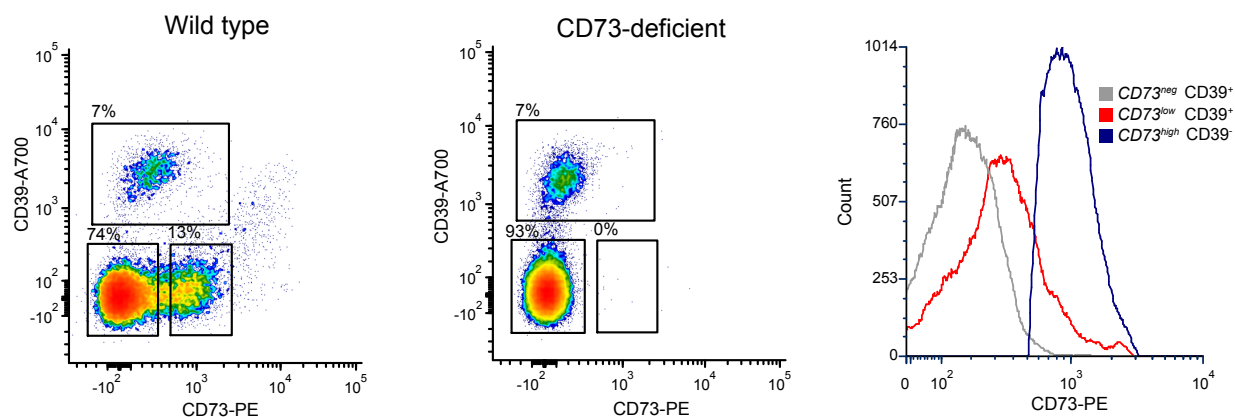
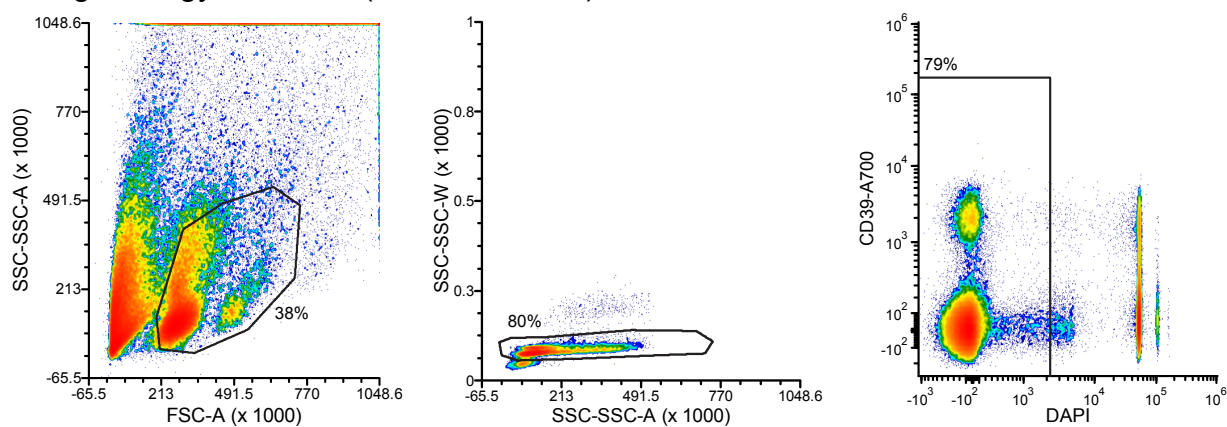
Membranes were cut prior to antibody staining to allow for simultaneous detection of proteins running at different sizes on the same membrane.

Supplementary Figure 3

Gating strategy for control ($CD73^{+/+}$) mice



Gating strategy for $Nt5e^{-/}$ ($CD73$ -deficient) mice

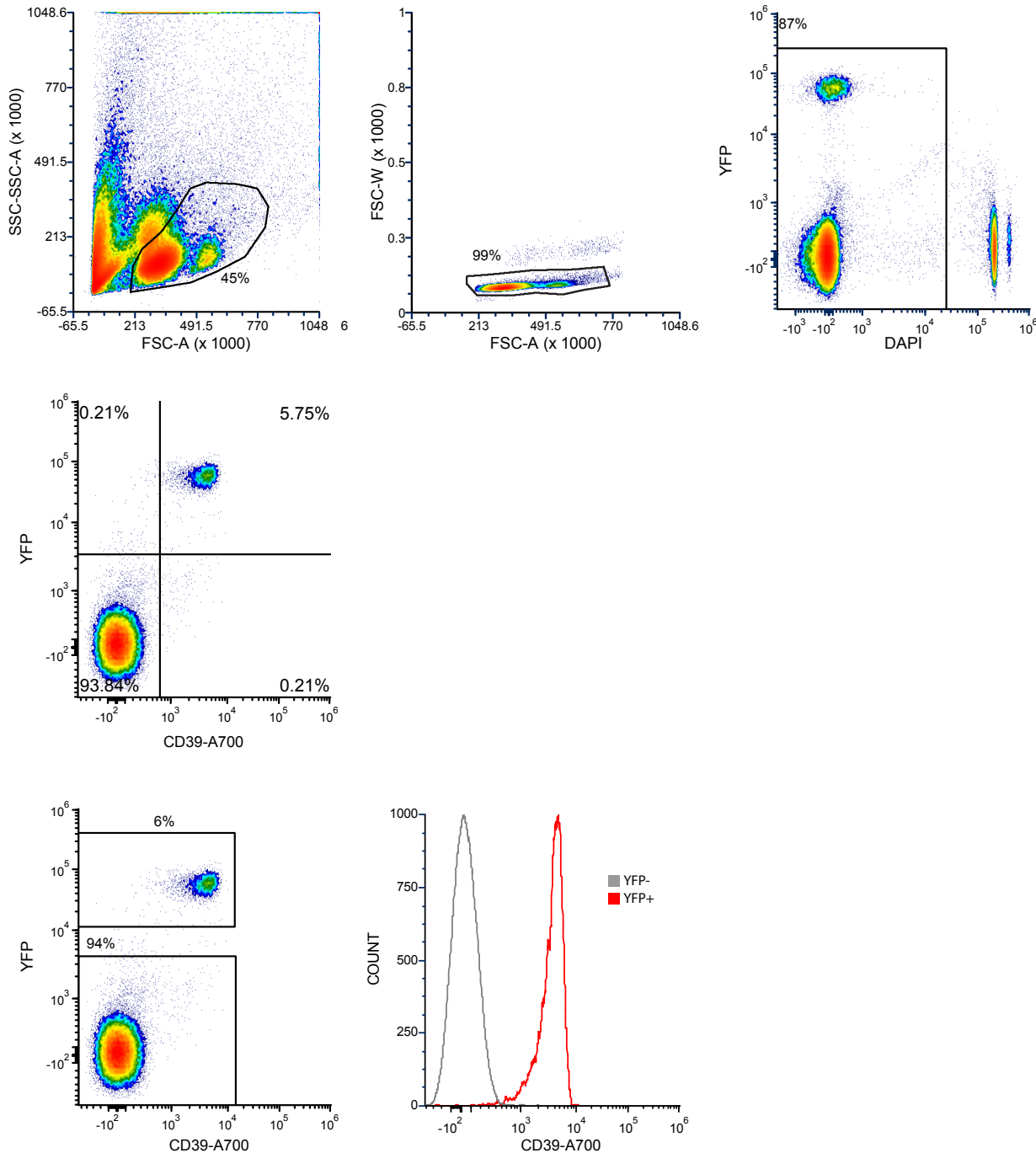


Gating strategy for Fig. 4b.

Compensation was performed on single-stained samples of UltraComp eBeads, unstained beads, and unstained cells. Forward and side scatter was used to gate on a defined population of cells to exclude debris and also select single cells. Live cells were determined as DAPI negative, as DAPI cannot penetrate through the membrane of live cells and thus was used to exclude dying/dead DAPI+ cells in the analysis. Gates were determined using unstained samples, fluorescence minus one (FMO) controls, in which one antibody was omitted per sample, isotype control for the CD73 antibody, and CD73-deficient $Nt5e^{-/}$ sample. Top row shows gating for control ($CD73^{+/+}$) mice. Middle row shows gating for mutant ($Nt5e^{-/}$ / $CD73$ -deficient) mice. Bottom row shows figures in main Fig. 4b.

Supplementary Figure 4

Gating strategy for full stained *Cx3cr1^{CreErt2/+}* (cytosolic YFP in microglia) brain, full stain

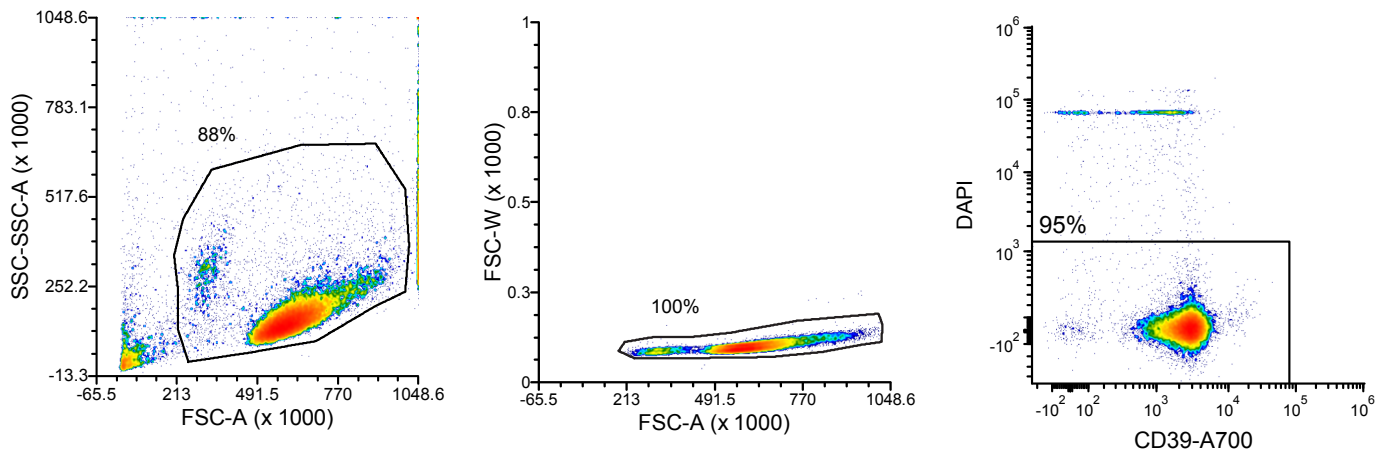


Gating strategy for Extended Data Fig. 7b.

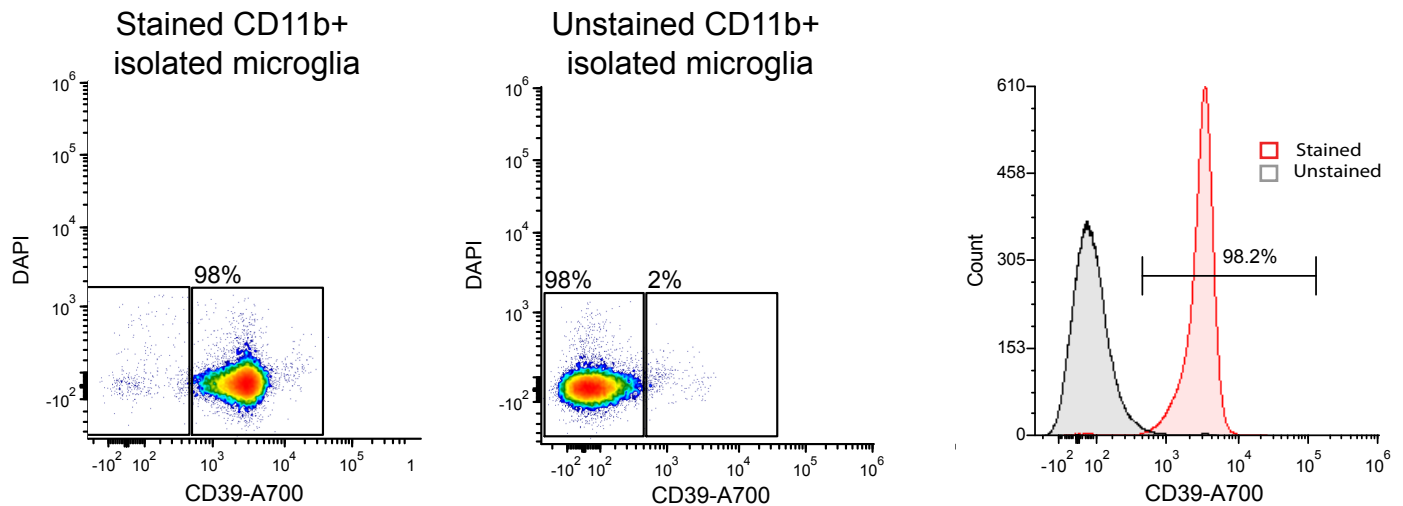
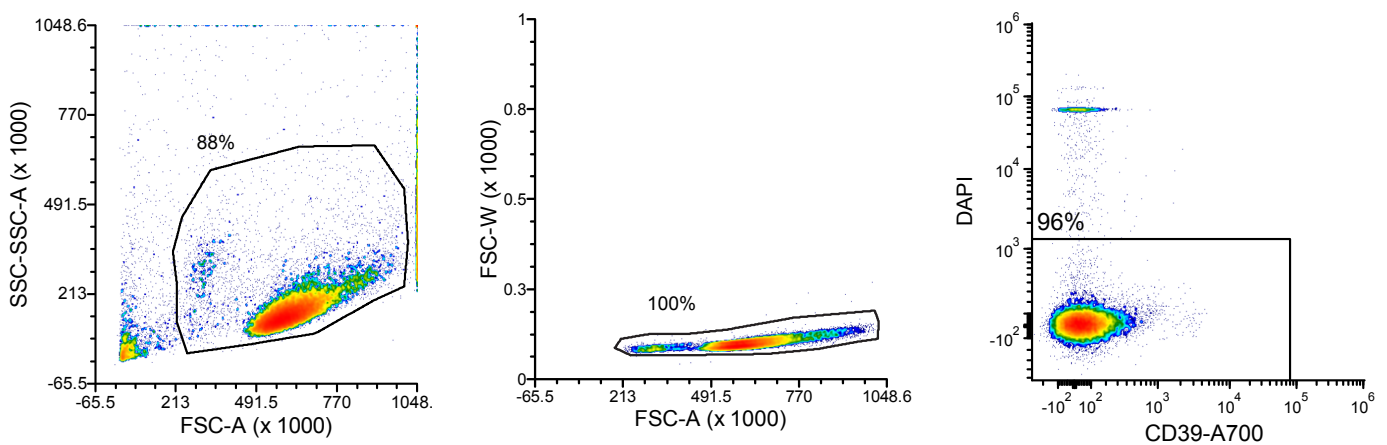
Compensation was performed on single-stained samples of UltraComp eBeads, unstained beads, YFP+ unstained brain (YFP only), and unstained cells. Forward and side scatter was used to gate on a defined population of cells to exclude debris and also select single cells. Live cells were determined as DAPI negative, as DAPI cannot penetrate through the membrane of live cells and thus was used to exclude dying/dead DAPI+ cells in the analysis. Gates were determined using unstained samples and fluorescence minus one (FMO) controls, in which one antibody was omitted per sample. Top row shows gating for *Cx3cr1^{CreErt2/+}* mice. Middle row shows percentages of CD39+ and CD39- cells based on YFP expression. Bottom row shows figures in Extended Data Fig. 7b.

Supplementary Figure 5

Gating strategy for full stained CD11b+ isolated microglia from neonatal pups



Gating strategy for unstained CD11b+ isolated microglia from neonatal pups



Gating strategy for Extended Data Fig. 7d.

Compensation was performed on single-stained samples of UltraComp eBeads, unstained beads, and unstained cells. Forward and side scatter was used to gate on a defined population of cells to exclude debris and also select single cells. Live cells were determined as DAPI negative, as DAPI cannot penetrate through the membrane of live cells and thus was used to exclude dying/dead DAPI+ cells in the analysis. Gates were determined using unstained samples and fluorescence minus one (FMO) controls, in which one antibody was omitted per sample. Top row shows gating strategy for stained CD11b+ isolated microglia. Middle row shows gating strategy for unstained CD11b+ isolated microglia. Bottom row shows figures in Extended Data Fig. 7d.

Supplementary Table 1

Genes enriched in striatal microglia upon neuronal activation (DESeq2, n=3 mice per group; *P* value < 0.05, fold change > 1.2) over unbound fraction (DESeq2, n=3/TRAP and unbound; *P* value < 0.05, fold > 2).

Supplementary Table 2

Genes enriched in striatal microglia upon neuronal inhibition (DESeq2, n=2 mice per group; *P* value < 0.05, fold change > 1.2) over unbound fraction (DESeq2, n=2/TRAP and unbound; *P* value < 0.05, fold > 2).

Supplementary Table 3

Genes enriched in D1 neurons in *Il34^{fl/fl}Drd1^{Cre/+}Drd1a^{TRAP}* mice over cre-negative littermate controls (DESeq2, n=3 mice per group; *p* value < 0.05, fold > 1.5) over unbound fraction (DESeq2, n=3 TRAP and 4 unbound; *p* value < 0.05, fold > 2).

Supplementary Video 1

Representative field of view for live imaging of calcium transients in striatal neurons for data shown in Figure 3a-f and Extended Data Figure 6a-g.

Supplementary Video 2

Representative field of view for live imaging of microglia (green) contact with neuronal terminals (red) for data shown in Figure 3g-h and Extended Data Figure 6h-j. Scale bar = 20µM.